Evaluation of Microfluidic Channels With Thin Si Windows and Trapping Structures

Masaya Toda, *Member, IEEE*, Hideki Hayashi, Nguyen van Toan, *Member, IEEE*, Naoki Inomata, and Takahito Ono, *Member, IEEE*

***Abstract*— We present the fabrication and evaluation of a microchannel with thin Si windows and a trapping structure for injected liquid samples, including an evaluation using tubing methods of polydimethylsiloxane eyelets, and Kovar. Yeast cells and latex particles were observed using a fluorescence microscope under atmospheric conditions and a scanning electron microscope (SEM) under vacuum. As moving and flowing liquid samples cannot be observed for a long time, a trapping structure in the microchannel is required. In our experiment using pole structures under a thin Si window in microchannels to trap liquid samples, we successfully observed them using the SEM under an accelerating voltage of 15 kV and an emission current of 75 μA. This result indicates the possibility of using higher accelerating voltages of electrons for higher observation resolutions at a lower power density of 2.3 kW/cm^2. Microfluidic channels with a thin window would be a useful technique for monitoring liquid samples under vacuum. [2020-0367]**

***Index Terms*— Microfluidic channel, SEM, cell observation, thin window, trapping structure.**

I. Introduction

CELLS that become cancerous can be distinguished from those that are about to die by changes in their surface shape and hardness [1]–[3]. Furthermore, changes in the nano-level resolution of cells that turn cancerous, observed over a span of a few minutes, can lead to the elucidation of the mechanism of cell death [4], [5]. A scanning electron microscope (SEM) is generally used in a vacuum environment to observe the microstructure and internal structure of objects or organisms; therefore, it is difficult to directly observe cells in a liquid [6]. Environmental scanning electron microscopy (ESEM) [7]–[9] and atmospheric scanning electron microscopy (ASEM) are used to observe biological samples such as liquids and cells [10]–[12]. In ESEM, the first electrons are generated in a high-vacuum environment, and the pressure around the sample is relatively close to the atmospheric pressure. On the other hand, the ASEM enables SEM observation by completely separating the liquid environment from the vacuum environment. This partition must be as thin as possible to transmit electron beams without reducing the resolution of the SEM. In previous studies, the observation of cells in a liquid using SEM was achieved by vacuum and liquid separation with a silicon nitride (SiN) thin film. A resolution of up to 8 nm was obtained using ASEM with a SiN thin-film window 30 nm thick [10]. Thus, the observation of adherent cells on the SiN thin film has been achieved using SEM, but the long-term observation of the suspended cells still faces certain drawbacks.

One of the drawbacks is the difficulty of observation using a commercially available SEM. In ESEM, pressure control in the chamber is indispensable. Therefore, it is necessary to make full use of the differential exhaust to create a pressure difference. Once the sample is placed on the stage and observation is initiated, it is inevitably carried out in a closed environment, making it difficult to keep a biological sample alive during the observation. For ASEM, it is necessary to set up the apparatus in an inverted form when compared to the traditional SEM because the sample is placed on a thin film dish. Therefore, a dedicated setup is required for ASEM.

On the other hand, magnetic resonance force microscopy (MRFM) is an imaging technique based on highly sensitive mechanical cantilever sensing with nanometer resolution [13]–[15]. Electron spin resonance (ESR)-MRFM has been developed for the 3D imaging of biological samples [16]–[18]. To apply MRFM to observe biological samples, the samples should be trapped at the location for a long time [17]. ESR-MRFM, which is operated in a high-vacuum environment, is a candidate for imaging biological samples based on radicals. Because the crystal defects in the SiN induce background noise for ESR-MRFM measurements, SiN might not be suitable as a window in the system.

In this study, a thin window made of single-crystal Si and a microchannel with a structure to trap floating specimens in liquid was constructed to enable long-term observation of the liquid samples. At the same time, the microchannels were compared using different tubing methods under atmospheric and vacuum conditions.

II. Working Principle and Designing

A. Device Concept

Fig. 1 shows the device concept of the proposed microfluidic channel with a thin window and a trapping pole in the microchannel. As the windows are thin, the first and second electrons of the SEM can pass through to enable observation of the inside of the microchannel. Si is preferred as the window material owing to its useful mechanical properties, such as

Manuscript received November 14, 2020; revised April 9, 2021; accepted April 27, 2021. Date of publication May 14, 2021; date of current version July 30, 2021. This work was supported in part by the Micro/Nanomachining Research Education Center (MNC) and the Micro System Integration Center (μSIC) of Tohoku University, in part by the Promotion of Joint International Research under Grant 15KK0225, in part by the KAKENHI under Grant 26706023, and in part by the Japan Society for the Promotion of Science (JSPS) under Grant 19H02568. Subject Editor C. Ahn. *(Corresponding author: Masaya Toda.)*

The authors are with the Graduate School of Engineering, Tohoku University, Sendai 980-8579, Japan (e-mail: mtoda@nme.mech.tohoku.ac.jp).

Color versions of one or more figures in this article are available at https://doi.org/10.1109/JMEMS.2021.3076791.

Digital Object Identifier 10.1109/JMEMS.2021.3076791

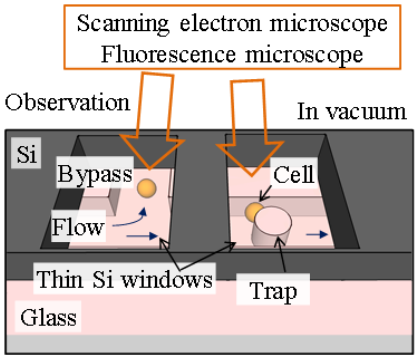

Fig. 1. Observation of liquid samples in microchannel with thin windows under vacuum.

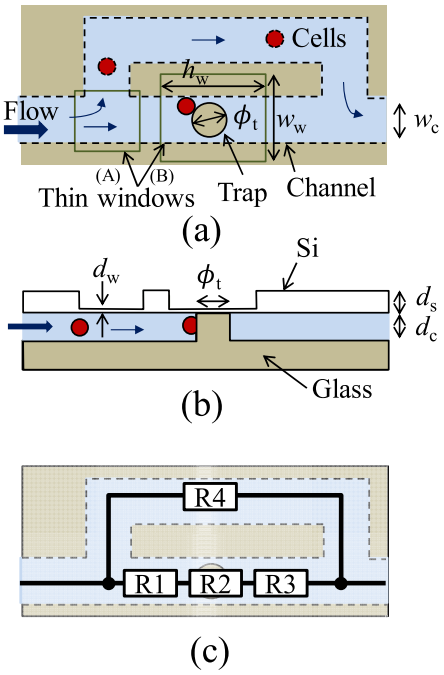

Fig. 2. Design of the microfluidic channel (a) top view and (b) side view, (c) equivalent circuit of the flow resistances.

high strength and crystalline structure. The device layer of a silicon-on-insulator (SOI) substrate has a single Si crystal without defects [19]. In the device concept, there are structures for trapping cells and branching of the liquid flow under the thin single-crystal Si window. Observation over a period of time using the SEM or optical microscopy from the top side was performed using trapping. The liquid, with the particle-like cells, flowed into the microchannel, and the pole in the microchannel trapped the specimens in the flowing liquid. The microchannel was separated into a trapping flow line using pole, and bypass lines. When a specimen is trapped at the pole, the branch part allows the liquid to flow towards the bypass owing to the inversion pressure difference, allowing the following sample to go to the bypass line.

B. Microchannel With Trapping Poles

Fig. 2 (a) and (b) show the top and side views of the device design for the proposed microfluidic channel. The specimen can be observed when it is trapped in the thin-film window in the microchannel. The depth (d_c) and width (w_c) of the microchannel were specified as 20 μm and 25 μm, respectively. Previous studies have shown that a 3.5 µm wide filter can trap more than 70 % of leukocytes [20]. In this study, we assumed that the target size of the specimen in the liquid was up to 10 μm. The distance of the gap between the pole and wall of the microchannel ranges between 2.5 μm and 10 μm. Therefore, the diameter (ϕ_t) of the pole was designed to be in the range of 5–20 μm. The designed number of trapping poles was 1–3. Owing to the tolerance of the microfabrication processes, various numbers of trapping poles were considered. The thickness (d_w) of the Si window was fixed at 200 nm, which is the thickness of the device layer of the SOI wafer. A thickness of 200 nm is thick enough to obtain sufficient production efficiency for the devices with windows with microchannels, and at the same time, it is sufficiently thin for observation, as shown in Table I. The size of the thin film window is limited owing to the effects of the stress generated by the differential pressure between the vacuum and the liquid, as discussed below. The thickness (d_s) around the thin window was set to the order of tens of micrometers. In a flow path with a trap structure, the flow path becomes clogged when the cells are trapped. Here, a structure was designed in which cells remaining in the liquid sample flow through a bypass flow path to the next trap structure.

TABLE I
ACCELERATION VOLTAGE AND PENETRATION DEPTH OF ELECTRONS IN SINGLE-CRYSTAL SILICON

Acceleration voltage[kV]	Free path length [µm]
5.0	0.3
10	1.0
15	2.0
20	3.2
25	4.8

Fig. 2 (c) shows a conceptual diagram of the bypass structure used in this design. The design was determined by calculating the pressure drop resulting from the resistance faced by the fluid from the wall surface of the flow path when the liquid was passed through. The pressure-drop Δp due to the resistance from the inner surface of the channel in the flow path is expressed by the following equation:

$$\Delta p = \frac{C(\alpha)}{32} \cdot \frac{\mu L Q P^2}{A^3}. \tag{1}$$

Here, $C(\alpha)$ is the coefficient determined by the friction loss coefficient and the Reynolds number with the aspect ratio α of the channel cross-section, μ is the fluid viscosity, L is the length of the channel, Q is the volumetric flow, P is the total length of the four sides of the cross section, and A is the cross-sectional area of the flow channel. Here, the pressure drop of the main flow with the trap part can be expressed as the sum of the three pressure drops, i.e., Δp_1 before the trap part, Δp_2 at the point of passing the trap part, and Δp_3 after the trap part. If the pressure drop in the bypass flow path

is Δp_b, the following relational expression can be obtained because the pressure drop is equal.

$$\Delta p_1 + \Delta p_2 + \Delta p_3 = \Delta p_b \tag{2}$$

The relationship among the pressure drops can be shown as an electric circuit by considering the pressure drop as a resistor, as shown in Fig. 2 (c) [21], [22]. If the flow rate of the main flow path is Q_1 and the flow rate of the bypass flow path is Q_2, the value of Q_1/Q_2 can be obtained from the equations. If $1 < Q_1/Q_2$, a large amount of the liquid flows towards the main flow path in the initial stage. As particles in a liquid tend to flow towards a path with a higher flow rate, it can be considered that the particles can be easily trapped under these conditions. In this study, we set $3 < Q_1/Q_2 < 4$ to ensure that the observation target flows towards the main flow path by designing ϕ_t between 5 μm and 20 μm using equation (1). The width of the bypass flow path was 25 μm, and the total length of the main flow path, apart from the trap part, was 145 μm.

C. Si Thin Window

In the ASEM that has already been developed, the size of the observation window of silicon nitride is 100 μm $\times$ 100 μm [10]. There is a limit to the size of the thin-film window that can withstand the differential pressure between the vacuum and liquid. In this study, single-crystal silicon was selected as the window material to separate the vacuum from the liquid. To determine the acceptable pressure, a yield stress of 1.8 GPa for a single-crystal silicon is considered. In particular, if the thin film window breaks while observing the liquid in the vacuum chamber, the liquid flows out into the vacuum chamber, which can adversely affect the vacuum pump. Therefore, in this study, we ensured that the stress generated in single-crystal silicon did not exceed 1.0 GPa. The pressure resistance and the allowable pressure are adjusted so that the thin film Si window with a 200 nm-thick film can withstand the differential pressure between the vacuum and the liquid. In our experiment, the liquid from the inlet was always sucked from the outlet side, so that the differential pressure between the vacuum and the liquid was assumed to be the atmospheric pressure. A uniformly distributed load was applied to a flat rectangular plate with four fixed sides.

The maximum stress σ_{max} is obtained from (3), where β is the ratio of the short side (a) to the long side, and p is the pressure applied to the window with a thickness of d_w [23].

$$\sigma_{max} = \beta \frac{pa^4}{d_w^2} \tag{3}$$

In this study, the channel width was 25 μm, and the thickness of the window was 200 nm. Two diaphragms with dimensions of (A) 50 μm $\times$ 50 μm and (B) 25 μm $\times$ 25 μm, respectively, were centered on the glass column for cell trapping. The maximum stresses were determined to be 430 MPa and 790 MPa, respectively, which are lower than the allowable stress.

The stress distribution on the window was also simulated using the finite element method, and COMSOL Multiphysics 4.4 software was used. The four sides of the window (50 μm $\times$ 25 μm) were fixed, and an atmospheric pressure of 1 atm was uniformly applied. The results are shown in Fig. 3. It was confirmed that the maximum stress was 711 MPa, which is similar to the calculated value and lower than the allowable value.

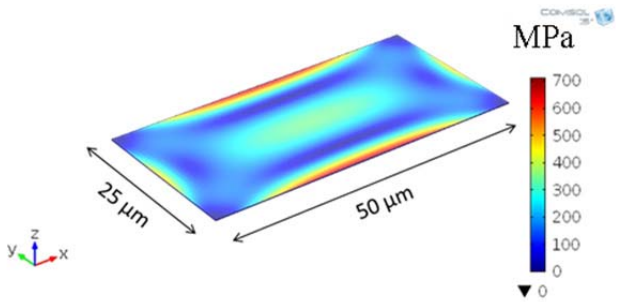

Fig. 3. Stress between atmosphere and vacuum in MPa.

D. Injection of Liquid

Three methods to inject liquid into microfabricated channels were considered in this research using a punched polydimethylsiloxane (PDMS) substrate, two glued eyelets, and Kovar substrates.

1) Simple Liquid Injection Using PDMS (Tubing Method 1): Liquid injection in the microfluidic device was performed using a punched PDMS substrate. Using the PDMS substrate with a premade hole, the rear sides of the glass and the PDMS substrate were attached to align the position of the hole for liquid injection. A relatively hard tube with an outer diameter slightly larger than the PDMS hole was connected as a fitting, and the liquid was injected using a syringe. PDMS connections were used to flow cells into the microchannel, as shown in Figs 6 (a) and 9 (a). Compared to other liquid injection methods using eyelets and Kovar, the PDMS method is the most popular and cheaper method. Conversely, because PDMS is permeable to gases [24], it causes an increase in pressure with a desirable thickness of 1 mm or more for tight tubing. Therefore, PDMS junctions are often used in conditions of atmospheric pressure.

2) Reliable Liquid Injection Using Eyelets (Tubing Method 2): In case a tighter fitting of inlet and outlet tubes is required, a glue method has been devised for the liquid injection process using eyelets [25]. In this report, the tubing method with eyelets was used in the prior evaluation for vacuum pumping, as shown in Fig. 6 (b), and it was found that a connection can be established with limited leakage (Fig. 7).

3) Less Leakage Injection Using Kovar (Tubing Method 3): In this study, a metallic substrate of Kovar with welded tubes was devised, and this mechanism was used for SEM image acquisition. Kovar is an alloy consisting of 29 % Ni and 17 % Co, and the remaining part is Fe. The advantage of using Kovar is that it is bonded with anodized glass, as shown in Fig. 6 (c). As previously reported, anodic bonding with glass can be performed, and it has been applied as an inlet for gases and liquids [26], [27]. The introduction of liquid or gas can be carried out in a high-pressure environment of 20 kPa with anode bonding in a narrow range. This bonding was

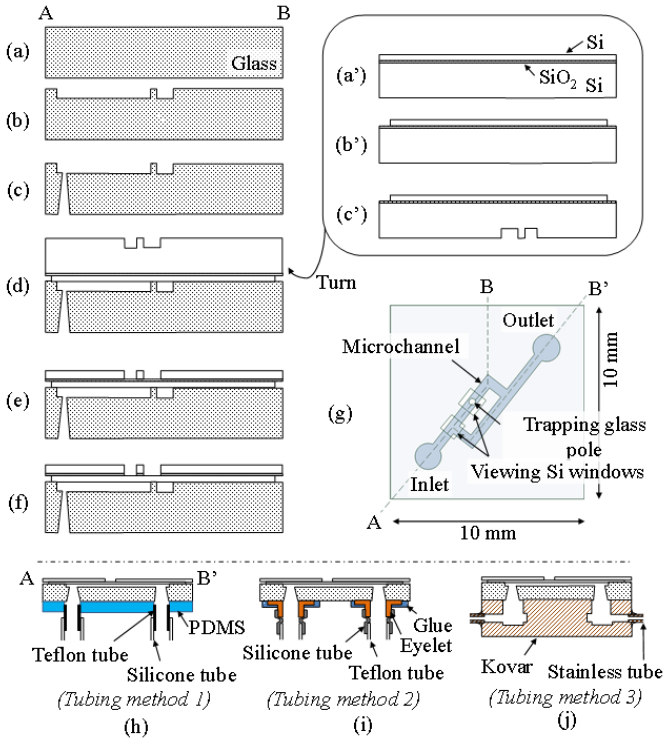

Fig. 4. Fabrication process of the device. (a) to (g) are cross-sectional views of the fabrication process, including the process bonded top part of (a') to (c'). (g) top view of the device design, and (h) to (j) are the used three tubing methods.

not affected by organic solvents. Therefore, it was considered suitable for the microfluidic channel in this study.

E. Fabrication

Fig. 4 shows the fabrication process of the proposed microfluidic channel with a thin Si window and a trapping pole below the window. A Si window was formed using the device layer of an SOI wafer. The size of the glass substrate was cut to a specification of 10 mm × 10 mm with a thickness of 300 μm (Fig. 4 (a)). For the glass etching, the reactive ion etching (RIE) method was used with an operational power of 100 W and a process pressure of 0.4 Pa using SF_6 gas (Fig. 4 (b)). A patterned Ni layer was used as the mask layer. To form the patterned Ni layer, sputtered Cr (20 nm thick) and Au (180 nm thick) were used as the seed layers for the electroplating of Ni. The thickness of the Ni layer was approximately 4 μm. After the electrodeposition of the Ni layer and removal of the photoresist, the seed layer of Cr-Au was etched through Xe ion milling (IBE-KDC75, Hakuto Co., Japan) with an operational power of 60 W and a process pressure of 0.4. The RIE process forms a microchannel and trapping pole in the channel [28]. Using a dry film resist (MS7050, Mitsubishi Paper Mill Ltd., Japan), the back end of the glass substrate was processed by a sandblast process (Sinto Kogio, Ltd., Japan) to form through holes (Fig. 4 (c)). Concurrently, to create a Si thin window, an SOI ($Si/SiO_2/Si$ = 0.2/0.4/300 μm, G6P-054-02, Soitec) wafer was prepared (Fig. 4 (a')). The Si layer around the top side was removed using CF_4/O_2 reactive etching of silicon with an operational power of 130 W and partial pressures of 90 Pa and 10 Pa for

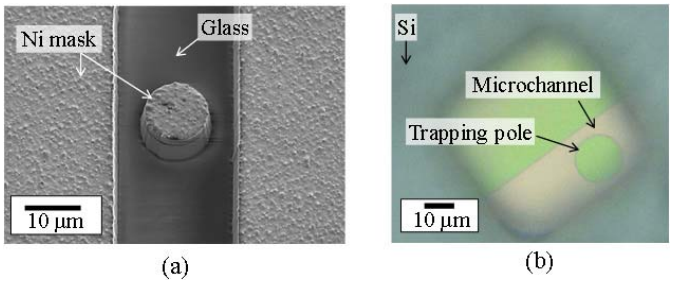

Fig. 5. (a) SEM image of the trapping part after the RIE process (Fig. 4 (b)), (b) optical image after the vapor HF etching (Fig. 4 (f)).

CF_4 and O_2, respectively (Fig 4 (b')). After the patterning of the photoresist on the handling layer side, the 30 μm-thick Si layer was etched by a deep RIE (MUPLX-SU2000, Sumitomo Precision, Japan) process (Fig. 4 (c')). The prepared glass substrate and processed SOI wafer were bonded using anodic bonding under atmospheric conditions (Fig 4 (d)). The entire surface of the handling Si layer of the SOI was then etched by the deep RIE process (Fig 4 (e)). Following vapor HF etching (Primaxx uEtch, SPTS), the insulation layer of SiO_2 was removed safely without any surface tension during the wet etching process (Fig. 4 (f)).

To evaluate the microfluidic chips, three tubing methods were used in this study to inject liquid samples. The fabrication details are presented below.

Tubing Method 1: One is the method of tubing using a PDMS layer with punched-through holes of 1 mm diameter. The surfaces of the PDMS and the glass become highly adhesive with the activated surfaces using a plasma cleaning machine (PIB-20, Vacuum Device, Japan) and were attached at high temperatures (between 100 °C and 150 °C), as shown in Fig. 4 (h).

Tubing Method 2: Two eyelets were used to form the tubing interface. A small amount of glue was used to attach the eyelet umbrella between the back of the device and the surface of the glass substrate (Fig. 4 (i)).

Tubing Method 3: Kovar metal that can perform bonding and can be anodized with glass. After drilling holes through the top and sides of the Kovar board, a stainless-steel pipe was welded into it to set up the pipe connection. After the bonding surface was polished to a mirror surface, the Kovar substrate was bonded to the glass substrate (Fig. 4 (j)).

F. Fabrication Results

Fig. 5 (a) shows the SEM image after the RIE process in the step shown in Fig. 4 (b). As such, it is an SEM image of Cr, Au, and Ni remaining on the glass. It may be possible to perform almost vertical etching, although the probability is low. Conversely, in many cases, the glass column is tapered by approximately 60–70°. The tapered structure has a higher flow resistance, which results in mostly flowing to bypass. In our experiments, the angle of the tapered structure could not be controlled by changing the RIE conditions. To clarify the details, further etching experiments for evaluation are required to obtain a higher fabrication yield with the vertical etching structure. Therefore, the 25 μm wide flow path pattern can be etched to a depth of 20 μm, but the 3 μm wide trap part pattern

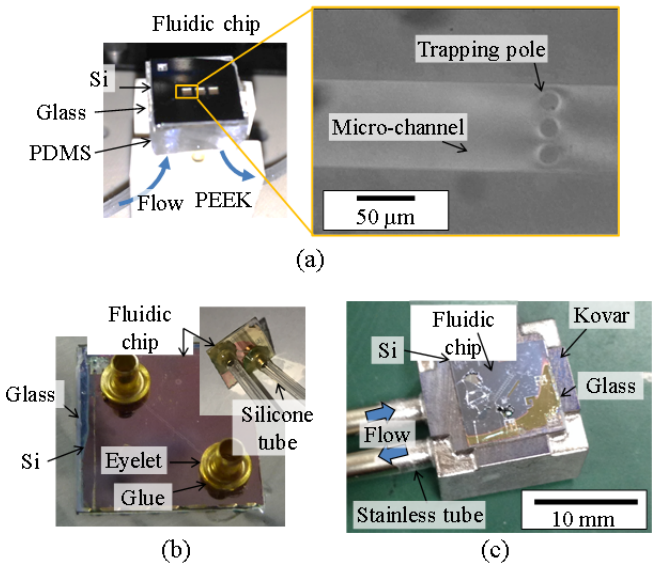

Fig. 6. After tubing, optical image of the channel with a thin Si window (a) using Tubing method 1 of PDMS, (b) using Tubing method 2 of eyelets, and (c) using Tubing method 3 of Kovar.

is etched only to a depth of several micrometers. Fig. 5 (b) shows an optical image obtained after the step shown in Fig. 4 (f). Because the bonded surface is clearly visible, it can be confirmed that the anode joint was successful.

Tubing Method 1: After attaching the PDMS substrate to the back of the glass, a Teflon tube (outer diameter 1.57 mm) and silicone tube (inner diameter 1 mm) were used for tube fitting. Because the PDMS hole diameter is 1 mm, it is possible to seal with minimal leakage by inserting a Teflon tube with an outer diameter of 1.57 mm. In addition, because a tube is attached to the back of the microfluidic device to introduce a liquid, a base was prepared using a polyether ether ketone (PEEK) stage to set the sample under an optical microscope, and the liquid introduction test and the cell observation experiment in the atmospheric environment were performed using this base (Fig. 6 (a)). The magnified image in Fig. 6 (a) shows the optical image of the microchannel and the trapping poles under a fluorescence microscope. A PEEK pedestal was used to introduce the tube into the fluorescence microscope. The liquid was introduced and discharged from the silicone tube and extended to the left and right sides. Fig. 6 (b) shows the liquid injection mechanism using the eyelets.

Tubing Method 2: The eyelets, with an outer diameter of 1.5 mm, inner diameter of 1.0 mm, umbrella diameter of 3.4 mm, and a height of 2.0 mm were attached to the back of the glass using adhesive. The figure on the right is a photograph of the connected silicone tube. After hardening, the silicone tubes (outer diameter, 1.5 mm; inner diameter, 1 mm) were fitted to the eyelets and connected (Fig. 6 (b)).

Tubing Method 3: The Kovar block, with a size of 15 mm × 15 mm × 10 mm, is bonded to the back side of the fluidic chip, as shown in Fig. 6 (c). In anode bonding, the flatness and surface roughness of the bonded surface are crucial. The surface roughness, Ra, was designed to be 50 nm in an area of 1 μm^2. Because the coefficient of linear expansion of

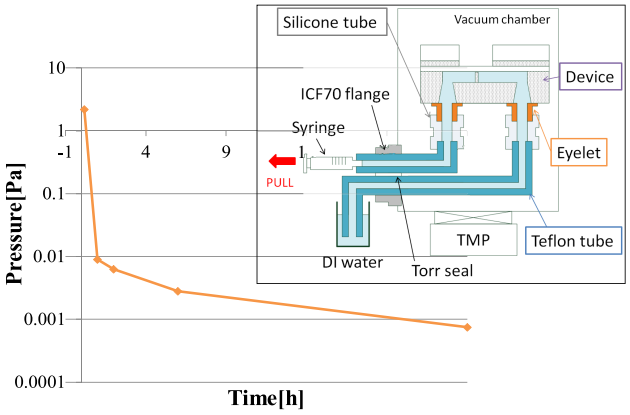

Fig. 7. Evaluation of vacuum test.

the Kovar and the glass is slightly different, the Kovar was designed to be larger than the glass, with less area on the top surface and with the cut edge as an alignment structure. The structure is designed such that the stress that can occur due to the difference in the coefficient of linear expansion can be released slightly after the cooling period in the anodic bonding process [27]. The Kovar, with a thickness of 10 mm, has holes with a diameter of 3.2 mm, and a stainless steel (SUS316Ls) pipe with a diameter of 1/8 inch were welded onto the side using a silver solder.

III. Experiments

A. Vacuum Pumping With Eyelets (Tubing Method 2)

A liquid injection mechanism was constructed using eyelets, and the feasibility of introducing a liquid into the microchannel was created to evaluate the sealing level for vacuum pumping. The experimental setup used in this study is shown in the inset of Fig. 7. Isopropyl alcohol (IPA), which has a low surface tension, is often used for liquid injection tests. Liquids with low surface tension are less susceptible to resistance from the tube during the introduction phase, which allows for rapid liquid injection. Because there is a risk that polymer-based glue, which is an organic substance, could be dissolved by IPA, a liquid injection test was conducted using de-ionized DI (deionized) water. The vacuum chamber used in this study can draw a vacuum of up to 6 × 10^{-5} Pa by connecting a turbo molecular pump.

First, the evacuation was performed with silicone tubes in a closed connection with the in/out Teflon tubes. In this case, the inner part of the microchannel was filled with air. At the beginning of the evacuation stage, the evacuation speed was low because gas was generated from the inner part of the silicone tube. In this experiment, it was confirmed that the evacuation speed was initially slow for approximately 10 min, but the vacuum pressure was drawn to a level of 10^{-4} Pa after approximately 2 h. DI water was then introduced into the microfluidic channel using a tube. The degree of vacuum over time is shown in Fig. 7. In the first 10 min, evacuation under vacuum was performed at a pressure of up to 2 Pa owing to the increase in the rotation speed of the turbo molecular pump and outgassing from the silicone tube. After 1 h, the vacuum pressure increased to 9 × 10^{-3} Pa, and it was considered that

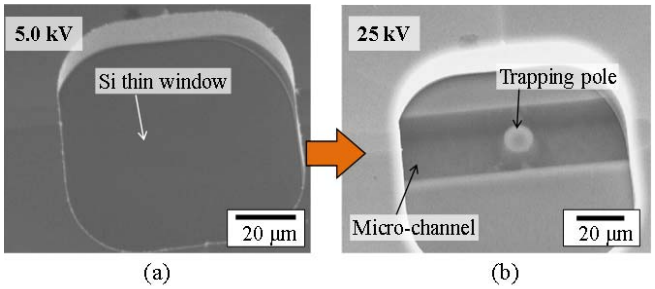

Fig. 8. SEM images of the microchannel at acceleration voltages of (a) 5 kV, (b) 25 kV.

most of the degassing was completed at this stage. After that, the degree of the vacuum pressure was gradually improved, and it was finally confirmed that the vacuum pressure could be increased to 7×10^{-4} Pa in the vacuum chamber for 24 h.

In this setup, it is observed that there is some leakage in either the tube-to-tube connection, the tube–eyelet connection, or the eyelet–device connection. As the silicone tube is gas permeable, it is possible that the leakage is due to the silicone tube. Based on this vacuum evaluation, it was confirmed that the microfluidic channel produced in this study can be applied to vacuum chambers such as scanning electron microscopes. However, gas leakage from the sample to create a high-pressure vacuum environment has drawbacks.

B. Evaluation of Thin Window

In the thin film Si window with a 200 nm thickness of the prepared microchannel, SEM observation is possible if an accelerating voltage above a certain value is applied. Thermionic SEM (S-2250N, Hitachi High-Technologies Co.) was used in this experiment. No liquid was introduced into the device, and the observation was performed in a dry state. The SEM images of the microchannel under accelerating voltage conditions of 5 kV and 25 kV are shown in Fig. 8 (a) and 8 (b), respectively. The SEM image was taken with the SEM stage tilted at 45°. As shown in Fig. 8 (a), the inside of the microchannel cannot be observed under an accelerating voltage of 5 kV, and only the surface of the thin film window was observed. When the accelerating voltage was raised to 25 kV, the electrons passed through the thin film window, as shown in Fig. 8 (b), and the surface of the glass column directly under the thin film window was observed. In addition, the interface between the bottom surface and the wall surface of the microchannel was confirmed.

C. Observation Results

1) Optical Observation: The cells were introduced into the microchannel and observed under a fluorescence microscope, as shown in Fig. 9 (a). For this evaluation, the cells were introduced using the PDMS tubing mechanism. All liquids were introduced under a negative pressure. Dry yeast (Kyoritsu Foods, Japan) was cultured at 36 °C with 50 mL of water and 5 mg of nutrient sucrose, for 3 h. The yeast was then stained with thiazole orange for fluorescence microscopy. The excitation light wavelength of the thiazole orange was 509 nm, and that of the fluorescence was 533 nm.

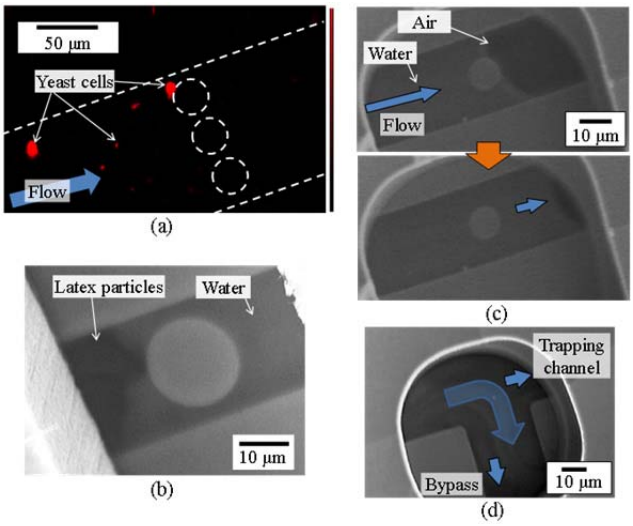

Fig. 9. (a) Yeast cells in microchannel observed by a fluorescence microscope and trapped with three trapping poles, and (b) latex particles trapped by single trapping pole, (c) a moving interface of the liquid and air, and (d) a branch point of the flow pass in the microchannel observed by a SEM with an acceleration voltage of 15 kV.

A microchannel with three trapping poles was used to trap the yeast cells. Fig. 9 (a) shows a fluorescence image of the yeast observed using a fluorescence microscope. It was observed that the yeast inside the flow path was trapped in the glass column within a few hours. From this observation, it was inferred that liquids and cells can be introduced into the microchannel, and that cells can be observed using a fluorescence microscope through a thin Si window.

2) Secondary Electron Observation: SEM observation was performed with the liquid passing into the microchannel with a single trapping pole. First, the thin film window was set at an accelerating voltage of 5 kV to ensure that the differential pressure did not break the thin window in the vacuum chamber. Here, latex particles in water (Micromer 6 μm, Micromod) were injected into the microchannel to evaluate the sample using SEM. By increasing the accelerating voltage to 15 kV, the electron beam passed through the thin film window made of single-crystal silicon, and latex particles in the liquid inside the channel were observed (Fig. 9 (b)). The emission current at this stage was 75 μA.

The interface of the liquid and air in the microchannel was observed, as shown in Fig. 9 (c). No liquid flowed on the right side of the glass column, whereas the left side was filled with liquid. In addition, as shown in Fig. 9 (d), the liquid at the branch point of the flow path branched. It was observed that the DI water moved with an air bubble in the microchannel. At an accelerating voltage of 20 kV or higher, the permeability of the electrons to the window increased, but the generation of bubbles was confirmed in the liquid inside the flow path.

Fig. 10 shows an image of the bubbles appearing in the flow path under the condition of an acceleration voltage of 25 kV and an emission current of 105 μA. After this stage, bubbles were generated on the right side of the column, and the liquid level returned to the vicinity of the thin film window. This was

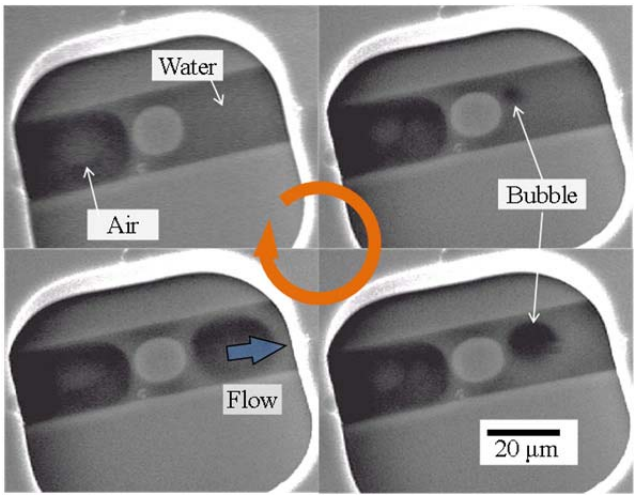

Fig. 10. SEM images of the bubbling in the channel (Acceleration voltage: 25 kV).

because the bubbles reached the branch point of the flow path and proceeded toward the bypass flow path side.

This phenomenon is presumably due to the fact that the temperature of the water inside the device rises locally owing to the energy of the electron beam and boils. Therefore, in a 200 nm Si thin-film window, it is desirable to observe cells with SEM under an accelerating voltage of less than 20 kV. The rate of generation of these bubbles increased as the magnification of the SEM observation increased, and when the magnification was lowered, the bubbles remained but did not expand. Although the expansion of the bubbles stops, the bubbles themselves do not disappear; therefore, it can be considered that the bubbles are generated due to the electron beam irradiation rather than the boiling temperature of the water.

D. Post-Observation

As shown in Fig. 9 (a), there were several yeast cells in the microchannel. To confirm the existence of the yeast cells in the channel, the inner part of the microchannel was observed again by SEM after removing the water from the microchannel, as shown in Fig. 11 (a). The width of the walls of the microchannel and the trapping pole is 4.5 μm, as shown in Fig. 9 (a). One of the poles trapped a few particles as a demonstration of our concept to trap the cells.

As shown in Fig. 9 (b), there are several latex particles of 6 μm in size. To confirm the existence of the particles, the inner part of the microchannel was observed again after removing the water from the microchannel. The SEM image in Fig. 11 (b) was then obtained, indicating that a very large number of latex particles were introduced into the microchannel. As shown in Fig. 9 (b), only a portion of the particles close to the thin window were observed considering the observational depth. The presence of the particles could not be confirmed in a liquid environment, but after the liquid was removed, a single latex particle was placed between the glass column and wall surface of the flow path, as shown in Fig. 11 (b). The wall width of the microchannel and trapping pole is 3.0 μm, as shown in Fig. 11 (b).

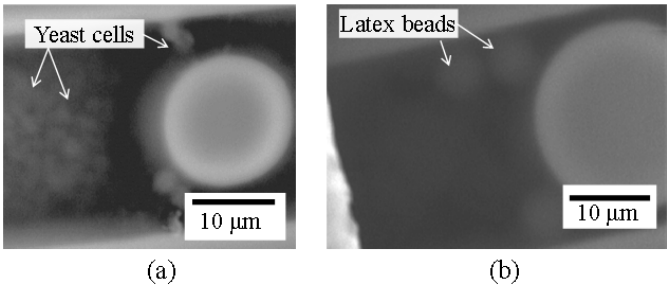

Fig. 11. SEM images of the inside of the microchannel without liquid (Acceleration voltage: 5 kV), (a) yeast cells and (b) latex particles.

IV. Discussion

A. Bubble Generation

Considering the influence of the electron beam on water, the generation of hydrogen bubbles from water can be explained by the following chemical reaction formula:

$$2H^{+}_{(\text{liquid})} + 2e^{-}_{(\text{electron beam})} \rightarrow H_{2(\text{gas})} \uparrow$$

If bubble generation results from high electron beam irradiation, it is considered that the generation of bubbles can be suppressed by lowering the emission current. During SEM observation with a higher emission current, the bubbles were frequently generated and expanded quickly, as shown in Fig. 10. When the emission current value was reduced below 90 μm from 105 μm, the expansion of the generated bubbles stopped, even under the condition of an accelerating voltage of 25 kV. In practical observations, the bubbles were not generated even under the conditions of an accelerating voltage of 25 kV and an emission current of 90 μm or less, regardless of whether the magnification was increased beyond the threshold point of bubble generation. Since the view area was 85 μm× 120 μm, the condition without bubble generation was less than 2.3 kW/cm^2 from our experiments. Therefore, it is possible to use a higher acceleration voltage with a lower emission current in the power density condition.

B. Observation Depth

It was found that the actual observable depth of the SEM was limited even if the observation was performed using a channel with a depth of 20 μm. Therefore, to observe the submerged sample in greater detail, it is crucial to bring the target sample to the vicinity of the thin-film window. The penetration depth of an electron beam into a substance can be estimated by finding the green range, which is the point at which the energy dissipation of the electrons becomes negligible. The green range R_G is calculated using the following equation from the sample density ρ and the kinetic energy E of the electrons [29]:

$$R_G = \frac{4 \times 10^5 \times E^{1.75}}{\rho}$$

From the equation, the penetration depth of electrons at the accelerating voltage used for this SEM observation is shown in Table I.

The electron beam passes through the thin window of a single-crystal silicon, collides with the pure water in the

microchannel, gets reflected, and is then detected through the thin window again. Even if the secondary electrons absorb all the energy of the primary electrons, they cannot pass through the thin film window at an accelerating voltage of 5.7 kV or less. The inner part of the flow path cannot be confirmed with an accelerating voltage of 5.0 kV. Even at an accelerating voltage of 10 kV, the secondary electrons of the water molecules that are actually emitted absorb only a part of the energy of the primary electrons, and the water inside the flow path could not be clearly observed. In this study, the surface of the liquid was observed by SEM, but the bottom surface of the flow path could not be observed through the liquid. As the penetration depth of the electron beam into water under an accelerating voltage of 25 kV is 11μm, the bottom surface of the flow path can be observed through the liquid by suppressing the depth of the flow path to approximately 5 μm. Conversely, the generation of bubbles was confirmed from the liquid at an accelerating voltage of 25 kV. This is presumably due to the high emission current, and it is surmised that observation at an accelerating voltage of 25 kV is possible by lowering the emission current.

V. Conclusion

Microchannel-type channels with a Si thin-film window and a thickness of 200 nm were prepared and introduced into a vacuum environment. The liquid was injected using three injection methods, and the sealing mechanisms were evaluated. PDMS tubing can be used under atmospheric conditions. The yeast cells flowed and were trapped successfully using the microfluidic channel. It was observed that the vacuum pressure could be drawn up to 1.6×10^{-3} Pa by evacuation for 2 h and up to 7.6×10^{-4} Pa by evacuation for 24 h using the eyelet tubing method. The tubing method using a bonded Kovar on Si was also a suitable method for observation under high-vacuum conditions. This study demonstrated that it is possible to separate the vacuum from the liquid using a 200 nm single-crystal silicon with a thickness that allows electron beams to pass through, and that it is possible to observe suspended cells in a liquid sample under a vacuum environment.

Using this device, the trapped specimens in the liquid sample were successfully observed using the SEM at an accelerating voltage of 15 kV and an emission current of 75 μA. The electron beam does not pass through the 200 nm Si thin-film window at an accelerating voltage of 5 kV, and it is possible to observe the inside of the flow path created by using an accelerating voltage of 15 kV or more. Conversely, when the accelerating voltage was raised to 25 kV, bubbles were generated from the water owing to the large amount of electron irradiation. This can be prevented by reducing the emission current. Higher accelerating voltages need to be used for higher resolution observations in the fluid using a lower power density of 2.3 kW/cm^2. In addition, an image of what appears to be a mass of latex particles was obtained, and the presence of latex particles was confirmed at that location after drying.

In our experiment using pole structures under a thin Si window in microchannels, the trapped specimens in liquid samples were successfully observed using the SEM. However, in SEM observation using a thermal electron source, there is a limitation to the resolution evaluation. Our result indicates the possibility of using higher accelerating voltages of electrons for higher observation resolutions at a lower power density of 2.3 kW/cm^2. The thin window of single-crystal Si shows the successful separation of liquid and high vacuum for further applications for observations of biological samples.

References

[1] S. L. Fink and B. T. Cookson, "Apoptosis, pyroptosis, and necrosis: Mechanistic description of dead and dying eukaryotic cells," *Infection Immunity*, vol. 73, no. 4, pp. 1907–1916, Apr. 2005.

[2] V. Janinová, T. Pereçko, J. Harmatha, R. Nosá, and K. Drábiková, "Decreased activity and accelerated apoptosis of neutrophils in the presence of natural polyphenols," *Interdiscipl. Toxicol.*, vol. 5, no. 2, pp. 59–64, Nov. 2012.

[3] D. V. Lebedev, A. P. Chuklanov, A. A. Bukharaev, and O. S. Druzhinina, "Measuring Young's modulus of biological objects in a liquid medium using an atomic force microscope with a special probe," *Tech. Phys. Lett.*, vol. 35, no. 4, pp. 371–374, Apr. 2009.

[4] F. Wang *et al.*, "Time resolved study of cell death mechanisms induced by amine-modified polystyrene nanoparticles," *Nanoscale*, vol. 5, pp. 10868–10876, Nov. 21 2013.

[5] G. Kroemer, B. Dallaporta, and M. Resche-Rigon, "The mitochondrial death/life regulator in apoptosis and necrosis," *Annu. Rev. Physiol.*, vol. 60, no. 1, pp. 619–642, Oct. 1998.

[6] S. E. Kirk, J. N. Skepper, and A. M. Donald, "Application of environmental scanning electron microscopy to determine biological surface structure," *J. Microsc.*, vol. 233, no. 2, pp. 205–224, Feb. 2009.

[7] A. M. Donald, "The use of environmental scanning electron microscopy for imaging wet and insulating materials," *Nature Mater.*, vol. 2, no. 8, pp. 511–516, Aug. 2003.

[8] Z. Zhang, Y. Zhou, X. Zhu, L. Fei, H. Huang, and Y. Wang, "Applications of ESEM on materials science: Recent updates and a look forward," *Small Methods*, vol. 4, no. 2, Feb. 2020, Art. no. 1900588.

[9] A. Bogner *et al.*, "A history of scanning electron microscopy developments: Towards 'wet-STEM' imaging," *Micron*, vol. 38, pp. 390–401, Dec. 2007.

[10] H. Nishiyama *et al.*, "Atmospheric scanning electron microscope observes cells and tissues in open medium through silicon nitride film," *J. Struct. Biol.*, vol. 169, no. 3, pp. 438–449, Mar. 2010.

[11] T. Yamazawa, N. Nakamura, M. Sato, and C. Sato, "Secretory glands and microvascular systems imaged in aqueous solution by atmospheric scanning electron microscopy (ASEM)," *Microsc. Res. Techn.*, vol. 79, no. 12, pp. 1179–1187, Dec. 2016.

[12] M. Sakaue, S. Miyoshi, and Y. Ominami, "Application of temperature controlled stage in atmospheric scanning electron microscopy," *Microsc. Microanal.*, vol. 23, no. S1, pp. 70–71, Jul. 2017.

[13] Y.-J. Seo, M. Toda, and T. Ono, "Si nanowire probe with Nd–Fe–B magnet for attonewton-scale force detection," *J. Micromech. Microeng.*, vol. 25, no. 4, Apr. 2015, Art. no. 045015.

[14] M. Li, H. X. Tang, and M. L. Roukes, "Ultra-sensitive NEMS-based cantilevers for sensing, scanned probe and very high-frequency applications," *Nature Nanotechnol.*, vol. 2, no. 2, pp. 114–120, Feb. 2007.

[15] F. R. Braakman and M. Poggio, "Force sensing with nanowire cantilevers," *Nanotechnology*, vol. 30, no. 33, Aug. 2019, Art. no. 332001.

[16] S. Tsuji, Y. Yoshinari, H. S. Park, and D. Shindo, "Three dimensional magnetic resonance imaging by magnetic resonance force microscopy with a sharp magnetic needle," *J. Magn. Reson.*, vol. 178, no. 2, pp. 325–328, Feb. 2006.

[17] S. Tsuji, T. Masumizu, and Y. Yoshinari, "Magnetic resonance imaging of isolated single liposome by magnetic resonance force microscopy," *J. Magn. Reson.*, vol. 167, no. 2, pp. 211–220, Apr. 2004.

[18] O. Záger, S. T. Hoen, C. S. Yannoni, and D. Rugar, "Three-dimensional imaging with a nuclear magnetic resonance force microscope," *J. Appl. Phys.*, vol. 79, no. 4, pp. 1881–1884, Feb. 1996.

[19] G. L. Pearson, W. T. Read, and W. L. Feldmann, "Deformation and fracture of small silicon crystals," *Acta Metallurgica*, vol. 5, no. 4, pp. 181–191, Apr. 1957.

[20] H. M. Ji, V. Samper, Y. Chen, C. K. Heng, T. M. Lim, and L. Yobas, "Silicon-based microfilters for whole blood cell separation," *Biomed. Microdevices*, vol. 10, no. 2, pp. 251–257, Apr. 2008.

[21] W.-H. Tan and S. Takeuchi, "A trap-and-release integrated microfluidic system for dynamic microarray applications," *Proc. Nat. Acad. Sci. USA*, vol. 104, no. 4, pp. 1146–1151, Jan. 2007.
[22] A. C. Rowat, J. C. Bird, J. J. Agresti, O. J. Rando, and D. A. Weitz, "Tracking lineages of single cells in lines using a microfluidic device," *Proc. Nat. Acad. Sci. USA*, vol. 106, no. 43, pp. 18149–18154, Oct. 2009.
[23] S. Timoshenko, *Theory of Plates and Shells*. New York, NY, USA: McGraw-Hill, 1959, pp. 396–428.
[24] A. Lamberti, S. L. Marasso, and M. Cocuzza, "PDMS membranes with tunable gas permeability for microfluidic applications," *RSC Adv.*, vol. 4, no. 106, pp. 61415–61419, 2014.
[25] K. Kawai, J. Uchikoshi, K. Arima, and M. Morita, "Nomally-closed valve integration for pneumatic actuators," in *Proc. 17th Int. Conf. Solid-State Sensors, Actuat. Microsyst.*, Jun. 2013, pp. 254–257.
[26] D. Y. Sim, T. Kurabayashi, and M. Esashi, "A bakable microvalve with a Kovar–glass–silicon–glass structure," *J. Micromech. Microeng.*, vol. 6, no. 2, pp. 266–271, Jun. 1996.
[27] M. T. Blom *et al.*, "Local anodic bonding of kovar to pyrex aimed at high-pressure, solvent-resistant microfluidic connections," *J. Micromech. Microeng.*, vol. 11, no. 4, pp. 382–385, Jul. 2001.
[28] X. Li, T. Abe, and M. Esashi, "Deep reactive ion etching of pyrex glass using SF6 plasma," *Sens. Actuators A, Phys.*, vol. 87, no. 3, pp. 139–145, Jan. 2001.
[29] T. E. Everhart and P. H. Hoff, "Determination of kilovolt electron energy dissipation vs penetration distance in solid materials," *J. Appl. Phys.*, vol. 42, no. 13, pp. 5837–5846, Dec. 1971.

Masaya Toda (Member, IEEE) received the Dr.Eng. degree from Osaka University, Japan, in 2007. From 2004 to 2007, he conducted research with the Max Planck Institute for Polymer Research, Germany. From 2008 to 2013, he was an Assistant Professor with the Graduate School of Engineering, Tohoku University, Japan, where he is currently an Associate Professor with the Department of Mechanical Systems and Design. He is also studying a nanomechanical observation system with magnetic resonance sensors for spin sensing applications in various fields. His research area is advanced sensing based on micro-and nano-mechanics.

Hideki Hayashi received the M.S. degree from Tohoku University, Japan, in 2015, where he is currently pursuing the master's degree with the Department of Mechanical Systems and Design. He started his research in micromechanical sensors at the School of Engineering, Tohoku University.

Nguyen van Toan (Member, IEEE) received the B.S. and M.S. degrees in physics and electronics from the University of Science, Vietnam National University, Ho Chi Minh City, Vietnam, and the Dr.Eng. degree from Tohoku University, in 2014, with a focus on silicon capable of integrating LSI for the application of timing devices. He is currently working as an Associate Professor with the Department of Mechanical Engineering, Graduate School of Engineering, Tohoku University. His current research interests include capacitive silicon resonators, optical modulator devices, capacitive micromachined ultrasonic transducers, thermal electric power generators, Knudsen pump, ion transportation, and metal-assisted chemical etching.

Naoki Inomata received the M.S. and Dr.Eng. degrees from Tohoku University, Sendai, Japan, in 2010 and 2013, respectively. From 2013 to 2016, he was an Assistant Professor with the Micro System Integration Center, Tohoku University. Since 2016, he has been an Assistant Professor with the Department of Mechanical Systems Engineering, Graduate School of Engineering.

Takahito Ono (Member, IEEE) received the Dr.Eng. degree from Tohoku University, in 1996. From 1996 to 2001, he was a Research Associate with the Graduate School of Engineering, Tohoku University, where he was an Associate Professor, from 2001 to 2009. From 2013 to 2016, he was a Professor with the Department of Mechanical Engineering, Graduate School of Engineering, University of Tokyo. He is currently a Professor with the Department of Mechanical Systems Engineering, Graduate School of Engineering, Tohoku University, where he is the Co-Director of the Micro System Integration Center. His research interests include microelectromechanical systems (MEMS), nanoelectromechanical systems, silicon-based nanofabrication, ultrasensitive sensing based on resonating devices, and the integration of functional materials into microsystems.